Secondary divertor heat loads during plasma current ramp down at high performance in ITER

M. Kočan[1], R. A. Pitts[1], Y. Gribov[1], R. Bruno[1], S. Carpentier-Chouchana[1], M. Firdaouss[2], A. A. Kavin[3], A. Loarte[1], V. E. Lukash[4], R. Mitteau[1],

[1] *ITER Organization, Route de Vinon sur Verdon, 13115 St Paul Lez Durance, France*

[2] *CEA, IRFM, F-13108 Saint Paul Lez Durance, France*

[3] *NIIEFA St. Petersburg, Russia,* [4] *RRC Kurchatov Institute, Moscow, Russia*

1. Introduction

During baseline $Q_{DT} = 10$ inductive operation in ITER, scenario designs with reliable vertical stabilization, but without invoking in-vessel vertical stabilization coils, require the plasma to be ramped down in H-mode from the plateau value of plasma current, $I_p = 15$ MA to approximately 10 MA [1]. However, as shown in Fig. 1, during the ramp down an upper X-point appears inside the first wall boundary. This may increase heat loads on the beryllium first wall panels (FWPs) [2], particularly on shaped regions of certain panels, or near gaps between panels, where field line incidence angle, α_{inc} can be relatively high.

This issue is addressed here by studying the full three dimensional upper divertor FWP loading during the plasma current ramp down using plasma configurations generated from the most recent DINA code [1] simulations. These new plasma ramp down configurations maximize the separation between the primary and secondary separatrices, Δ_{sep}, keeping the parallel heat fluxes at the first contact points with the wall as low as possible. Heat fluxes are imposed assuming that edge localized modes (ELMs) will be controlled during ITER burning plasma operation and that they will carry the majority of the power exhausted into the far scrape-off layer (SOL). The focus will be on the power loads to the upper FWPs during two potentially problematic ramp down phases depicted in Fig. 1: (i) the early (~full bore) phase characterized by $I_p = 15$ MA, when the upper strike point appears near the FWP 8 and the power (P_{SOL}) circulating in the SOL plasma is relatively large, and (ii) the phase at $I_p = 12.3$ MA when the strike point crosses the toroidal gap between FWPs 8 and 9.

2. Main wall power fluxes during ELMs

A full model of the ELM power deposition on the main wall, q_{depELM} which would self-consistently describe the formation, detachment and propagation of filaments during ELMs is not currently available. An estimate for q_{depELM} is thus obtained here through a simple and adhoc 'power balance' model [3], based on present experimental evidence and understanding of the ELM transients. The maximum ELM-averaged parallel heat flux density in the SOL at the outboard mid-plane (OMP) secondary separatrix is estimated as

$$\langle q_{// ELM} \rangle = \Delta W_{ELM}(W/W_0) f_{ELM}/(2 n_{fil} \lambda w_{fil})/1.7 = \Delta W_{ELM}(W/W_0) f_{ELM}/(n_{fil} \lambda d)/1.7, \quad (1)$$

where ΔW_{ELM} is the plasma energy loss per ELM, W/W_0 is the fraction of the initial energy in a single ELM filament which reaches the secondary separatrix, f_{ELM} is the ELM frequency, λ is the ELM filament energy decay length at the secondary separatrix, n_{fil} is the number of filaments per ELM, w_{fil} is the poloidal filament FWHM and $d = \ell_{out}/(n_{fil} q_{edge})$ is the poloidal separation of the filaments (with $\ell_{out} \approx \pi \langle a \rangle$ the poloidal length over which the ELM filaments cross the secondary separatrix on the plasma outboard side), assuming $w_{fil} = d/2$ [4]. The numerical factor 1.7 in Eq.(1) accounts for the fact that the filaments strike the FWPs at random toroidal locations but can overlap. In case of the largest overlap (i.e. the maximum ELM-averaged heat load), the heat load to the FWPs is reduced by 1.7 compared with the heat load that would arise if all filaments were to strike at the same toroidal location [3].

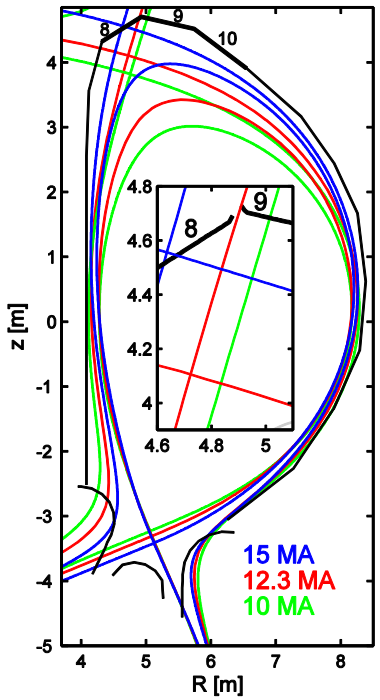

Fig.1. Poloidal cross-section of ITER showing the separatrices during the plasma current ramp down in H-mode. Inset shows the upper strike point position. Numbers indicate the FWPs.

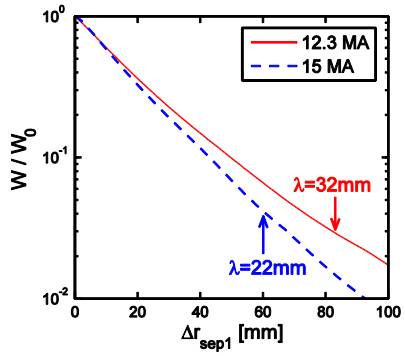

Fig.2. Fraction of the ELM filament energy evaluated from the parallel loss model versus the primary separatrix distance at the OMP. Arrows: secondary separatrix.

Table 1 compiles the other main parameters important for the power load simulations: at I_p = 15 MA, P_{SOL} = 100 MW, and the maximum allowed size of controlled ELMs is $\Delta W_{ELM} \approx 1$ MJ [3]. This gives $f_{ELM} = P_{ELM}/\Delta W_{ELM} = 40$Hz, assuming $P_{ELM} \approx 0.4 P_{SOL}$ which is an upper limit for the power convected from the confined plasma by controlled ELMs in ITER [3]. The same considerations for $I_p = 12.3$ MA ($\Delta W_{ELM} \propto I_p^{1.25} \approx 1.3$ MJ and $P_{SOL} = 71$ MW due to lower α-particle heating $\propto I_p^3$) give $P_{ELM} = 28$ MW and $f_{ELM} = 22$ Hz.

A fluid model of the parallel ELM filament transport in the SOL [5] is used to estimate W/W_0 and λ. For specified initial filament temperatures and density, the model computes the time evolution of these quantities due to parallel transport to the nearest surface. Current understanding of the ELM cycle is insufficient to provide theory-based estimates for the location in the pedestal plasma from which any given ELM filament is ejected into the SOL. We proceed under the conservative assumption that they originate from the primary separatrix, with T_i, T_e and n_e characteristic of half the values at the pedestal top (Table 1). In the model, temporal and radial evolution of the ELM filament parameters are coupled through the radial filament speed, v_r. Here v_r = constant = 500 m s^{-1} is assumed, corresponding to the largest anticipated v_r for controlled ELMs in ITER [3]. The values of W/W_0 and λ obtained from the model are shown in Fig. 2 (see also Table 1), together with $\langle q_{// ELM} \rangle$ estimated from Eq. (1) accounting for the magnetic flux expansion at the upper FWPs (which increases the value at the OMP by a factor ~1.7).

3. Secondary divertor heat loads

The field line tracing code PFCFlux [6] has been used to calculate q_{depELM} at the upper FWPs 8-10, with the latter represented by triangular meshes. The meshes were obtained directly from CAD models of the current shaping design for the FWPs [2]. These FWPs are designed such that a staggered arrangement allows the avoidance of any field line penetration down to shield block steel edges. A section of the model is shown in Fig. 3. For the 15 MA equilibrium, q_{depELM} is maximum on FWP 8 which intersects the secondary strike point. At 12.3 MA, the highest power load is found on FWP 9, which is in the vicinity of the secondary strike point and outside the private flux region. Other FWPs included in the field line tracing model act as magnetically shadowing objects. Artificial 'ridges' (not shown in Fig. 3) were placed in the rear of each FWP to eliminate

I_p [MA]	15	12.3
ΔW_{ELM} [MJ]	1	1.3
P_{SOL} [MW]	100	71
f_{ELM} [Hz]	40	22
$n_{e\,ped}$ [10^{19} m^{-3}]	7.5	6.2
$T_{i\,ped} = T_{e\,ped}$ [keV]	5	4.1
Δ_{sep} [mm]	60	83
W / W_0	4.2	3
λ [mm]	22	32
$\langle q_{//\,ELM} \rangle$ [MW/m^2]	7	2.4
n_{fil}	10	10
q_{edge}	3	3
ℓ_{out} [m]	10	10

Table 1. Numerical values considered for the controlled ELM heat load specifications during the plasma current ramp down in ITER for two different values of I_p.

unphysical plasma-wetted areas due to the field lines striking from behind FWPs. Starting from each grid node on the FWP surface contour, field lines are followed for up to 10 m. The node is flagged as magnetically shadowed if intersection occurs on any FWP surface within this distance. Figure 4d illustrates that in the magnetic shadow the parallel connection length $L_{//} < 2$m, so that the ELM filaments dilute within a radial distance $\approx L_{//} v_r / c_s \approx$ mm with the sound speed $c_s \approx 10^5$ m s^{-1}. This makes it reasonable to neglect q_{depELM} in the magnetic shadow ($q_{depELM} = 0$ is also imposed in the private flux region and outside the secondary separatrix in the high field side SOL which is magnetically disconnected from ELM filaments in the low field side SOL). For each of the plasma-wetted nodes,

$$q_{depELM} = (R_{OMP}/R_{loc}) \cdot \sin(\alpha_{inc}) \cdot \langle q_{//\,ELM} \rangle \cdot \exp(-\Delta r_{sep2}/\lambda), \quad (2)$$

where R_{loc} and Δr_{sep2} are, respectively, the local major radius and the distance from the secondary separatrix mapped to the OMP. The total power deposited on the FWP, q_{dep} includes q_{depELM}, the heat flux due to plasma radiation (at most 0.35 MWm^{-2}) and accounts for heat flux 'penalties' due to manufacturing tolerances and the details of the FWP design omitted in the model [2]. As shown in Fig. 5, at $I_p = 15$ MA, the maximum $q_{dep} \approx 2.3$ MW/m^2 which is a factor 2 below the power handling capability of the upper FWPs (4.7 MWm^{-2}) [2]. In order to study the sensitivity of q_{dep} on FWP 9 to variations in secondary strike point position around the gap between FWP 8 and 9, the 12.3 MA equilibrium was shifted outwards by $\Delta_{out} = 0$-9 cm relative to the strike point position shown in Fig. 1. In Fig. 6, the deposited power averaged over 1 cm^2 receiving the largest power load, q_{depmax}, is plotted against Δ_{out}. In Fig. 6, the deposited power averaged over 1 cm^2 receiving the largest power load, q_{depmax}, is plotted against Δ_{out}. For $\Delta_{out} \approx 0$-50 mm, the surface heat fluxes are highest in

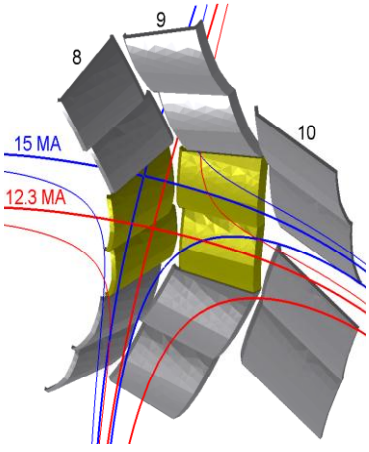

Fig. 3. Section of the model of the FWPs 8-10. Also shown are the separatrices and the flux surface characterized by 1/e of the ELM heat flux at the secondary separatrix. The studied FWPs are highlighted.

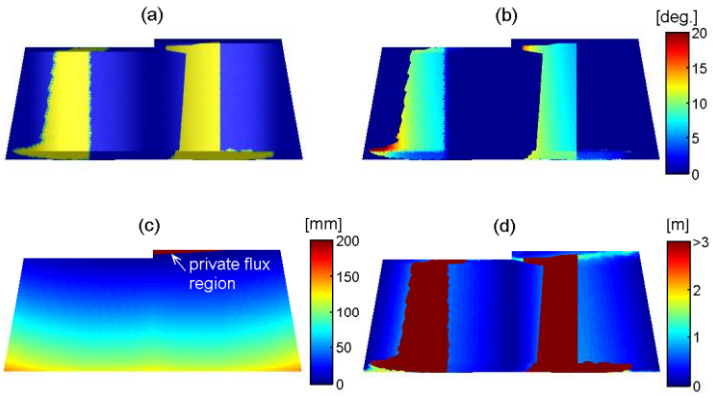

Fig. 4. (a) Plasma-wetted area, (b) field line incidence angle in the plasma-wetted area, (c) distance from the 2nd separatrix mapped to the OMP and (d) the parallel connection length in the magnetically shadowed area of the FWP 9 at $I_p = 12.3$ MA.

Fig. 5. FWP 8 surface heat flux at I_p = 15MA.

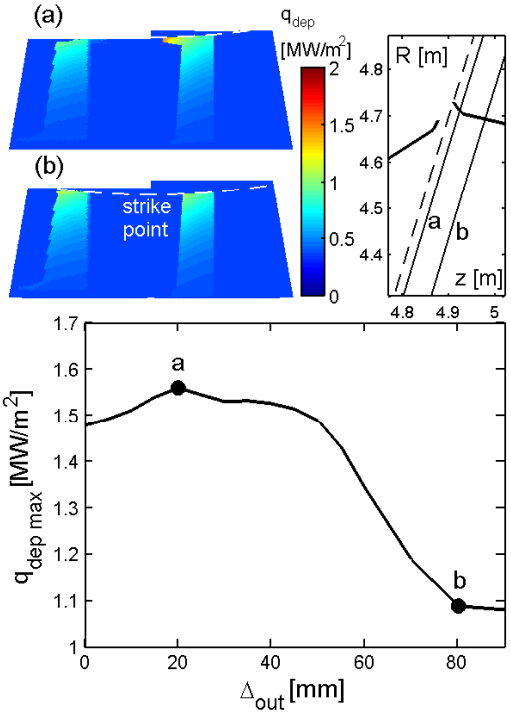

Fig. 6. Bottom: deposited power averaged over 1cm^2 surface of the FWP 9 receiving the highest power, calculated for different secondary strike positions Δ_{out}. Top panels show q_{dep} on the FWP 9 for (a) Δ_{out} = 20 mm and (b) Δ_{out} = 80 mm. Upper right: corresponding secondary strike point positions (dashed: Δ_{out} = 0).

the area (dubbed 'hot spot') located near the poloidal panel offset, where α_{inc} is relatively large and Δr_{sep2} is small (Figs. 4 and 6). For Δ_{out} = 0-20 mm, q_{depmax} increases as the strike point moves closer to the hot spot and eventually reaches the hot spot location. However, the poloidal flux expansion yields a high value of λ in the secondary divertor region (Fig. 3), so that the shift of the strike point towards the hot spot has only weak effect on q_{depmax}. For Δ_{out} = 20→80 mm, $q_{dep\ max}$ decreases as the private flux region overlays the hot spot location, and remains constant for Δ_{out} > 80 mm. The largest $q_{dep\ max}$ is a factor 3 below the steady state power handling capability of FWP 9. Note that the ELMs would produce tolerable heat loads even if the filaments were propagating in the primary SOL with v_r up to ~1 km s^{-1} – a factor 2 larger than with the largest v_r anticipated for controlled ELMs in ITER. This provides some margin given the large uncertainties in the expected v_r.

4. Summary

The study here demonstrates that the expected surface heat fluxes in the nominal current ramp down scenario for ITER Baseline Q_{DT} = 10 inductive operation will be well within the power handling margins of the upper FWPs. The heat fluxes are a factor 2 lower than the power handling margin in the early full-bore ramp down phase and a factor 3 lower when the secondary strike point crosses the gap between the FWPs 8 and 9.

Disclaimer: The views and opinions expressed herein do not necessarily reflect those of the ITER Organization.

References

[1] V. M. Leonov et al., Proc. 37th EPS Conference on Plasma Phys. 2010, Dublin, Ireland, P2.182.
[2] R. Mitteau, et al., Fusion Engineering and Design, 2012 (submitted).
[3] A. Loarte et al., Proc. 22nd Int. Conf. on Fusion Energy 2008 (Geneva, Switzerland, 2008) (Vienna: IAEA) IT/P6-13.
[4] N. Ben Ayed et al., Plasma Phys. Control. Fusion **51** (2009) 035016.
[5] W. Fundamenski and R. A. Pitts, Plasma Phys. Control. Fusion **48** (2006) 109.
[6] M. Firdaouss et al., J. Nucl. Mater. **438** (2013) S536.